Appl Phys B (2008) 93: 389–401
DOI 10.1007/s00340-008-3215-z

Applied Physics B
Lasers and Optics

Initial wavefunction dependence on atom interferometry phases

M.A.H.M. Jansen · K.A.H. van Leeuwen

Received: 11 February 2008 / Revised version: 30 July 2008 / Published online: 3 October 2008

Abstract In this paper we present a mathematical procedure to analytically calculate the output signal of a pulsed atom interferometer in an inertial field. Using the well-known $ABCD\xi$ method we take into account the full wave dynamics of the atoms with a first order treatment of the wavefront distortion by the laser pulses. Using a numerical example we study the effect of both the length of the beam splitting laser pulses and of the width of the initial spatial distribution of the atoms. First, we find that in a general inertial field the interferometer only has a limited window in terms of the initial width (centered around 100 μm in the example calculation) in which interference fringes are visible at all. This effect is caused by the inevitable statistical spread in atomic parameters, such as initial position and momentum, and the dependence of the interferometer phase on these. In the optimum case, the useful range of the initial width is formed by the range in which both the spatial distribution and the diffraction limited momentum spread are small enough to avoid large phase differences over the atomic wavefunction. As a second result we find that the interferometer phase depends strongly on the length of the laser pulses and, to a smaller extent, on the initial width of the atomic cloud. This spatial dependency is relatively small ($\sim 10^{-5}$ rad) and justifies semiclassical approximations, as used in other calculations, for most experiments. New high-accuracy experiments, however, will come in the range where this effect is no longer negligible.

PACS 37.25.+k · 03.75.-b · 03.65.Fd

M.A.H.M. Jansen (✉)
Harvard University, 17 Oxford street, 02138 Cambridge, MA, USA
e-mail: jansen@hussle.harvard.edu

K.A.H. van Leeuwen
Eindhoven University of Technology, P.O. box 513, 5600MB Eindhoven, The Netherlands
e-mail: K.A.H.v.Leeuwen@tue.nl

1 Introduction

Atom interferometers have proven to be an accurate and versatile tool for measuring a large range of physical phenomena [1, 2], ranging from gravity [3, 4] and rotation [5–7] to atomic properties like transition frequencies [8–10] and electric polarizabilities [11, 12]. Building upon the successes of the past, new and even more precise interferometers are being built that are designed specifically to test: fundamental constants, such as the fine structure constant [13] and the gravitational constant [14, 15], principles of physics, such as the equivalence principle [16], and general relativistic effects, like the Lense–Thirring and geodetic effects [17].

As the precision of the measurements is increased, however, more and more effects have to be taken into account [18] that influence the interferometer signal and thereby distort the outcome of the measurement (for beamsplitter effects see, e.g., [19, 20]). Usually, the interferometer phase is calculated only for the center of the atomic wave using a very simplified model of the atom beam splitters. These simplifications then ignore the wavefront distortion (dispersive effect) by the beamsplitter on the atomic wave. However, it is well known that a deformation of the wavefront can lead to imperfections in the interference signal and an effective phase shift of the fringes. The goal of this paper is to do a full quantum mechanical calculation of the interference signal that does include this dispersion by the beamsplitter. For

this we will largely follow the methods that have been described in, e.g., [21] and [22], but with additions to improve the validity range and the possibility of obtaining analytical expressions.

In this paper we will consider two parameters that affect the final interferometer phase: the laser pulse length τ and the width of the initial atomic wavefunction $\sigma_{r,0}$. The effect of τ has been studied in the past (see, e.g., [4, 19, 20, 22, 23]) for cases that wavefront distortion effects are neglected. However, the dynamics change if dispersion is present and the final interferometer phase is different. The effect of $\sigma_{r,0}$, or the shape of the initial wavefunction in general, has not been calculated systematically before. We now show that the choice of the initial atomic cloud does have an effect on the measured interferometer phase at a level that may be detectable with proposed experiments. Although non-dispersion theories have worked very well so far, the calculations in this paper show that the full atomic wavefront distorting effect of the laser pulses can no longer be neglected for future high-precision interferometers.

The layout of the paper is as follows. We start, in Sect. 2, by calculating the quantum mechanical propagator of the atomic wave. The setup that we consider in this paper is a pulsed Mach–Zehnder configuration in a rotating reference frame (corresponding to a frame fixed to the rotating surface of the Earth) and a quadratic potential. As an example of such a potential we will use the second order expansion of the local gravitational field. First, we perform a series of transformations to an interaction picture with respect to the inertial motion and the unperturbed Rabi oscillations of the atom beamsplitters. The resulting Schrödinger equation only contains the cross terms that are caused by the chirped Doppler shift during the interaction with the lasers. These effects are usually very small because of the short lengths of the laser pulses and the relatively slow chirp and we can use a series expansion of the final evolution operator. Then, in Sect. 3, we explain how the resulting propagator is evaluated and how the interferometer phase is obtained. Although the solution is analytical, in principle, it is very extensive and we use a numerical example based on the proposal in [16]. The results of the calculations are given in Sect. 4, where we show the behavior of both the interference contrast and the phase as a function of the pulse length and the size of the initial atomic sample. We will show that there is a limited range of initial atom cloud sizes that actually give visible interference fringes and that the measured phase does depend on both the length of the laser pulses and the initial cloud size.

2 Theory

2.1 Framework

In this work we will describe the interference signal in the case that the evolution of the atomic wavepacket is determined by a Hamiltonian that has three contributions:

$$\hat{H}_{\text{tot}} = \hat{H}_0 + \hat{H}_{\text{ext}}(\hat{\boldsymbol{r}}, \hat{\boldsymbol{p}}) + \hat{H}_{\text{laser}}(\hat{\boldsymbol{r}}, t), \tag{1}$$

where $\hat{\boldsymbol{r}}$ is the (3D) position operator and $\hat{\boldsymbol{p}}$ is the momentum operator. Another approach that has been very successful in calculating interferometer phases is the use of pathintegrals [24–26]; however, it is very difficult to describe the effect of laser pulses in this formalism. The internal energy levels are given by $\hat{H}_0$ and the interaction with the laser pulses by $\hat{H}_{\text{laser}}(\hat{\boldsymbol{r}}, t)$. The center of mass motion is described by [27]:

$$\hat{H}_{\text{ext}} = \frac{\hat{\boldsymbol{p}}^2}{2m} - m\boldsymbol{g}\cdot\hat{\boldsymbol{r}} - \frac{m}{2}\,\hat{\boldsymbol{r}}\cdot\overrightarrow{\Gamma}\,\hat{\boldsymbol{r}} - (\hat{\boldsymbol{r}} + \boldsymbol{R})\cdot\overrightarrow{\Omega}\,\hat{\boldsymbol{p}}, \tag{2}$$

where we limit ourselves to a Hamiltonian that is maximally quadratic in momentum and position. In the case of gravity, $\boldsymbol{g}$ is the gravitational acceleration, but, in general, $m\boldsymbol{g}$ is the gradient or the first order expansion term of the potential field around the origin of the coordinate system. The second order expansion terms of the potential are described by $m\overrightarrow{\Gamma}/2$, where the matrix $\overrightarrow{\Gamma}$ can, e.g., represent the gravity gradient. Equation (2) is the Hamiltonian in a rotating coordinate system that has an origin which is separated by the vector $\boldsymbol{R}$ from a point on the axis of rotation (see Fig. 1). An example of such a situation is a setup that is fixed to the surface of the rotating earth. The rotation term is described by the matrix $\overrightarrow{\Omega}$:

$$\overrightarrow{\Omega} = \begin{pmatrix} 0 & \Omega_z & -\Omega_y \\ -\Omega_z & 0 & \Omega_x \\ \Omega_y & -\Omega_x & 0 \end{pmatrix}, \tag{3}$$

such that

$$\boldsymbol{r}\cdot\overrightarrow{\Omega}\,\boldsymbol{p} = -\boldsymbol{r}\cdot\boldsymbol{\Omega}\times\boldsymbol{p} = \boldsymbol{\Omega}\cdot\boldsymbol{r}\times\boldsymbol{p} \tag{4}$$

gives the usual rotational energy term. We use this matrix notation instead of the usual vector notation because matrix multiplications are easier to perform and handle than vector cross-products.

We will model the atom as a two-state system. The laser pulses are modeled to have a single frequency and uniform intensity in space. Then in the interaction picture with respect to $\hat{H}_0$ and using the rotating wave approximation

$$\hat{H}_0 + \hat{H}_{\text{laser}}(\hat{\boldsymbol{r}}, t) = \frac{\hbar}{2}\Omega_R(t)\begin{pmatrix} 0 & e^{i(\boldsymbol{k}\cdot\hat{\boldsymbol{r}}+\Delta_l t+\phi_l)} \\ e^{-i(\boldsymbol{k}\cdot\hat{\boldsymbol{r}}+\Delta_l t+\phi_l)} & 0 \end{pmatrix}, \tag{5}$$

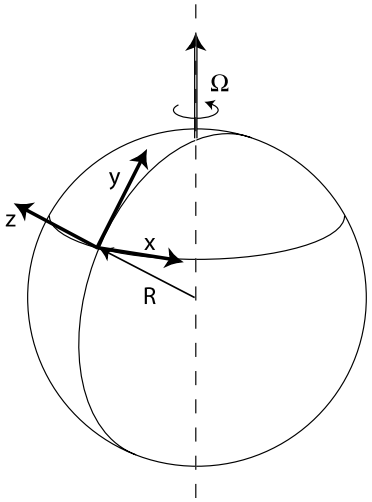

Fig. 1 Schematic representation of the used coordinate system. The origin is located at the entrance of the interferometer which is fixed to the surface of the rotating Earth

where $\Omega_R(t)$ is the (space independent) Rabi frequency, $\boldsymbol{k}$ is the laser wavevector, $\Delta_l = \omega_l - \omega_0$ is the laser detuning and ω_l and ϕ_l, respectively, are the frequency and the offset phase of the laser. The energy difference of the upper state with the lower state is $\hbar\omega_0$ and we ignore any spontaneous emission. This model can be used whenever the energy differences with all other states are large in comparison with the laser detuning. One example is the case when the laser is tuned to resonance with an atomic transition. However, often multi-photon processes, like Raman transitions [28] and Bragg scattering [29], can also be described as an effective two-level system.

2.2 *ABCDξ* transformations

Because the laser pulses are short compared to the total time lapse of the interferometer sequence, the largest contribution to the interferometer phase originates from $\hat{H}_{\text{ext}}$. We can then simplify the calculations by switching to an interaction picture with respect to this part of the Hamiltonian. Bordé showed [21, 30, 31] that the resulting total Hamiltonian in this picture can be written as:

$$\hat{H}'_{\text{tot}} = \hat{H}_0 + \hat{H}_{\text{laser}}\left(\vec{A}\,(t)\hat{\boldsymbol{r}} + \vec{B}\,(t)\hat{\boldsymbol{p}} + \boldsymbol{\xi}(t), t\right), \tag{6}$$

where the (3×3) matrices $\vec{A}\,(t)$, $\vec{B}\,(t)$, $\vec{C}\,(t)$, and $\vec{D}\,(t)$ are the solution to the differential equation

$$\frac{d}{dt}\begin{pmatrix}\vec{A} & \vec{B}\\ \vec{C} & \vec{D}\end{pmatrix} = \vec{M}\begin{pmatrix}\vec{A} & \vec{B}\\ \vec{C} & \vec{D}\end{pmatrix} \tag{7}$$

with the initial condition

$$\begin{pmatrix}\vec{A} & \vec{B}\\ \vec{C} & \vec{D}\end{pmatrix}_{t=0} = \begin{pmatrix}1 & 0\\ 0 & 1\end{pmatrix} \tag{8}$$

and where $\vec{M}$ is the 6×6 matrix

$$\vec{M} \equiv \begin{pmatrix}\vec{\Omega} & 1\\ \vec{\Gamma} & \vec{\Omega}\end{pmatrix}. \tag{9}$$

The vectors $\boldsymbol{\xi}(t)$ and $\boldsymbol{\zeta}(t)$ follow the differential equations

$$\begin{aligned}\frac{d}{dt}\begin{pmatrix}\boldsymbol{\xi}\\ \boldsymbol{\zeta}/m\end{pmatrix} &= \vec{M}\begin{pmatrix}\boldsymbol{\xi}\\ \boldsymbol{\zeta}/m\end{pmatrix} + \begin{pmatrix}\vec{\Omega}\,\boldsymbol{R}\\ \boldsymbol{g}\end{pmatrix},\\ \begin{pmatrix}\boldsymbol{\xi}\\ \boldsymbol{\zeta}/m\end{pmatrix}_{t=0} &= \begin{pmatrix}0\\ 0\end{pmatrix}.\end{aligned} \tag{10}$$

We would like to note that the classical trajectories are given by

$$\boldsymbol{x}_{\text{cl}}(t) = \vec{A}\,(t)\boldsymbol{x}_0 + \vec{B}\,(t)\boldsymbol{p}_0 + \boldsymbol{\xi}(t). \tag{11}$$

Transformation (6) is thus the quantum-mechanical equivalent of a reference frame that moves along the classical atomic trajectory. The classical momentum in the rotating coordinate system is given by

$$\boldsymbol{p} = m\left(\boldsymbol{v} - \vec{\Omega}\,(\boldsymbol{r}+\boldsymbol{R})\right), \quad \boldsymbol{v} = \frac{d\boldsymbol{r}}{dt}. \tag{12}$$

If $\vec{\Omega}$ and $\vec{\Gamma}$ are time-independent, it is possible to find an exact solution to (7), (8) and (10). Furthermore, the rotation rate and the gravity gradient are usually sufficiently small compared to the time scale T of the experiment ($\|\vec{\Omega}\|T \ll 1$, $\|\vec{\Gamma}\|T^2 \ll 1$) to allow a series expansion in time [32]. In that case

$$\begin{pmatrix}\vec{A} & \vec{B}\\ \vec{C} & \vec{D}\end{pmatrix} = e^{\vec{M}t} = 1 + \vec{M}\,t + \frac{1}{2!}\vec{M}^2\,t^2 + \cdots, \tag{13}$$

$$\begin{aligned}\begin{pmatrix}\boldsymbol{\xi}\\ \boldsymbol{\zeta}/m\end{pmatrix} &= \vec{M}^{-1}\left(e^{\vec{M}t} - 1\right)\begin{pmatrix}\vec{\Omega}\,\boldsymbol{R}\\ \boldsymbol{g}\end{pmatrix}\\ &= \left(t + \frac{1}{2!}\vec{M}\,t^2 + \frac{1}{3!}\vec{M}^2\,t^3 + \cdots\right)\begin{pmatrix}\vec{\Omega}\,\boldsymbol{R}\\ \boldsymbol{g}\end{pmatrix}\end{aligned} \tag{14}$$

2.3 Laser interaction

With the transformations of the previous section we get the Hamiltonian in the interaction picture with respect to $\hat{H}_{\text{ext}}$ and $\hat{H}_0$:

$$H'_{\text{tot}} = \frac{\hbar}{2}\begin{pmatrix}0 & \Omega_R e^{i\hat{\phi}(t)}\\ \Omega_R e^{-i\hat{\phi}(t)} & 0\end{pmatrix}, \tag{15}$$

with

$$\hat{\phi}(t) = \boldsymbol{k} \cdot \left(\overrightarrow{A}(t)\hat{\boldsymbol{r}} + \overrightarrow{B}(t)\hat{\boldsymbol{p}} + \boldsymbol{\xi}(t)\right) - \Delta_l t + \phi_0. \tag{16}$$

If we can derive a propagator from this Hamiltonian, we can easily write down the evolution operator of the entire multi-pulse interferometer sequence. Unfortunately, except for the simple case of a linear potential [33, 34], this is impossible because of the fact that the operator $\hat{\phi}(t)$ involves the two non-commuting operators $\hat{\boldsymbol{r}}$ and $\hat{\boldsymbol{p}}$. Therefore, we will have to make some approximations to calculate the interference signal. We will assume that the phase change during the pulses is very small and that the effect of the pulses is well approximated by an unperturbed Rabi oscillation. We then move to an interaction picture with respect to this unperturbed Rabi oscillation and calculate the (small) deviation from this in a perturbative manner.

There are two characteristic features about the Rabi oscillations: the oscillation of the atomic population between ground and excited state and the imprint of the laser phase on the wavefunction of the excited state [28]. We will treat these features separately, for clearer notation further on. We account for the laser phase imprint using the transformation

$$\hat{U}_1(t) = \begin{pmatrix} e^{i\hat{\phi}(t)} & 0 \\ 0 & 1 \end{pmatrix}, \tag{17}$$

which leaves the Hamiltonian

$$\hat{H}_1 = \hbar \begin{pmatrix} \frac{d\hat{\phi}(t)}{dt} & \Omega_R/2 \\ \Omega_R/2 & 0 \end{pmatrix}. \tag{18}$$

Next we go to a system that rotates with the unperturbed Rabi oscillation, starting when the laser pulse is turned on at t_0 ($t' = t - t_0$, which we will mostly evaluate at the end of the pulse $t' = \tau$)

$$\begin{aligned} \hat{U}_2(t') &= e^{-\frac{i}{2}\begin{pmatrix} 0 & \Omega_R \\ \Omega_R & 0 \end{pmatrix} t'} \\ &= \begin{pmatrix} \cos(\Omega_R t'/2) & -i\sin(\Omega_R t'/2) \\ -i\sin(\Omega_R t'/2) & \cos(\Omega_R t'/2) \end{pmatrix} \\ &\Downarrow \end{aligned} \tag{19}$$

$$\hat{H}_2 = \hbar \frac{d\hat{\phi}(t)}{dt} \begin{pmatrix} \cos^2(\frac{\Omega_R}{2}(t-t_0)) & -\frac{i}{2}\sin(\Omega_R(t-t_0)) \\ \frac{i}{2}\sin(\Omega_R(t-t_0)) & \sin^2(\frac{\Omega_R}{2}(t-t_0)) \end{pmatrix}. \tag{20}$$

The changes by this remaining Hamiltonian are very small ($\tau d\hat{\phi}/dt \ll 1$) and we approximate the remaining evolution by

$$\hat{U}_3(t_0, t') = 1 + \frac{1}{i\hbar}\int_{t_0}^{t_0+t'} \hat{H}_2(t)\, dt + \cdots. \tag{21}$$

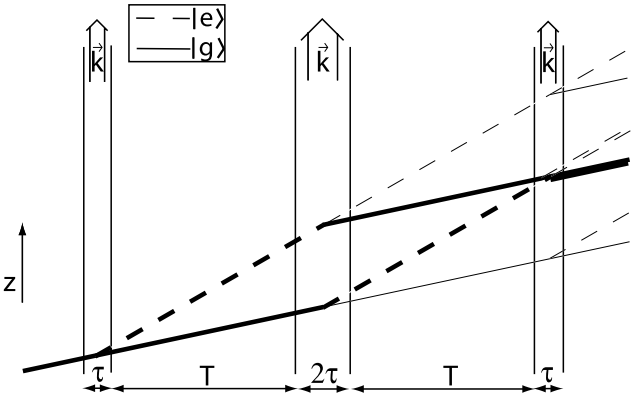

Fig. 2 Schematic representation of the pulse sequence in the Mach–Zehnder configuration. Inertial effects, such as gravity and rotation, are omitted from the trajectories for clarity. Two paths that form an interference signal are indicated by the *thick lines*

The effect of one single laser pulse is then given by [1]

$$\hat{U}_{\text{laser}}(t_0, \tau) = \hat{U}_1(t_0 + \tau)\hat{U}_2(\tau)\hat{U}_3(t_0, \tau)\hat{U}_2^{-1}(0)\hat{U}_1^{-1}(t_0), \tag{22}$$

which for the moment we will write as

$$\begin{pmatrix} e^{i\hat{\phi}(t_0+\tau)}\hat{U}_{ee}(t_0,\tau)e^{-i\hat{\phi}(t_0)} & e^{i\hat{\phi}(t_0+\tau)}\hat{U}_{eg}(t_0,\tau) \\ \hat{U}_{ge}(t_0,\tau)e^{-i\hat{\phi}(t_0)} & \hat{U}_{gg}(t_0,\tau) \end{pmatrix}. \tag{23}$$

In this form only the main contributions of the phases are written down explicitly and the transition amplitudes combined with the corrections to the phase are summarized in the operators $\hat{U}_{ij}$. Note that this is all still written in terms of operators that do not commute, so that the two exponentials in the upper diagonal element cannot be simply combined.

2.4 Atom interferometer

In this work we consider a perfectly symmetric Mach–Zehnder interferometer (see Fig. 2). The atoms enter the interferometer in the ground state with some initial velocity. The first laser pulse ($\pi/2$) with length τ excites the atoms to an equal superposition of the excited and the ground state. The excited state has acquired a momentum difference of $\hbar k$ and spatially separates from the ground state. At the point of maximum separation, at $t = T + \tau$, a second laser (π) pulse of length 2τ inverts the distribution over the internal states and the associated momentum. The two spatially separated parts of the wavefunction get back together. At $t = 2T + 3\tau$, a third pulse of length τ is given, which mixes the two parts of the wavefunction. The fraction of atoms in the ground state is then a measure of the phase difference between the

[1] Note that we use the interaction picture of $\hat{U}_1$ and $\hat{U}_2$ only temporarily and transform back at the end of each laser pulse.

two paths. When all phase shifts of, e.g., gravity and rotation as well as the dispersive effects of the laser pulses are neglected, all atoms will exit the interferometer in the ground state.

As indicated in the figure, the total interferometer signal is actually an interference of 4 different paths (per internal level). However, the second π pulse can be tuned very accurately so that the occupation of the two "extreme" paths (upper and lower paths at the end of the interferometer in Fig. 2) is very small. Furthermore, these two paths are spatially separated from the two classically overlapping paths. If the spatial wavefunctions are located sufficiently, there is no overlap and the interference effects from these two paths can be neglected. The two extreme paths then only introduce an offset in the signal, which we will ignore in the following calculations.

With the propagator during the laser pulses (cf. (23)) we can calculate the atomic wavefunction at the end of the interferometer sequence. Because in the interaction picture with respect to $\hat{H}_{\text{ext}}$ the wavefunction does not change between pulses, the final wavefunction is simply given by the evolution during the laser pulses. The total interferometer propagator is then a product of several matrices $\hat{U}_{\text{laser}}$ with the appropriate starting time and pulse length. If one is interested in the actual spatial structure of the wavefunction, one has to apply the inversion of the transformations in Sect. 2.2. However, in a pulsed atom interferometer, the number of atoms in an internal state is usually measured, averaging over a large detection region. In that case, information on the spatial distribution is lost and we do not need these inverted transformations.

The total interferometer signal of a Mach–Zehnder configuration is given by the propagator:

$$\hat{U}_{MZ} = \hat{U}_{\text{laser}}(2T+3\tau,\tau)\hat{U}_{\text{laser}}(T+\tau,2\tau)\hat{U}_{\text{laser}}(0,\tau). \tag{24}$$

In the two-path approximation, we manually set the diagonal terms of the second matrix to zero, resulting in, e.g., the lower diagonal element (see Appendix A):

$$\hat{U}_{MZ,gg} = e^{-i\hat{\phi}_3^0} e^{i\hat{\phi}_2^+} \left(\hat{g}_1 + e^{-i\hat{\phi}_{MZ}}\hat{g}_2\right), \tag{25}$$

where

$$\begin{aligned}\hat{\phi}_{MZ} = {} & \hat{\phi}_1^+ - \hat{\phi}_2^0 - \hat{\phi}_2^+ + \hat{\phi}_3^0 \\ & - \frac{i}{2}\left(\left[\hat{\phi}_2^+, \hat{\phi}_3^0\right] + \left[\hat{\phi}_2^0, \hat{\phi}_1^+\right] - \left[\hat{\phi}_2^+ - \hat{\phi}_3^0, \hat{\phi}_1^+ - \hat{\phi}_2^0\right]\right),\end{aligned} \tag{26}$$

$$\begin{aligned}\hat{g}_1 = {} & \hat{U}_{ge}^3\left(\hat{\boldsymbol{r}} + \hbar\left(\overrightarrow{B}_3^0 - \overrightarrow{B}_2^+\right)^T\boldsymbol{k}, \hat{\boldsymbol{p}} - \hbar\left(\overrightarrow{A}_3^0 - \overrightarrow{A}_2^+\right)^T\boldsymbol{k}\right) \\ & \times \hat{U}_{eg}^2(\hat{\boldsymbol{r}},\hat{\boldsymbol{p}})\hat{U}_{gg}^1(\hat{\boldsymbol{r}},\hat{\boldsymbol{p}}),\end{aligned} \tag{27}$$

$$\begin{aligned}\hat{g}_2 = {} & \hat{U}_{gg}^3\left(\hat{\boldsymbol{r}} + \hbar\left(\overrightarrow{B}_2^0 - \overrightarrow{B}_1^+\right)^T\boldsymbol{k}, \hat{\boldsymbol{p}} - \hbar\left(\overrightarrow{A}_2^0 - \overrightarrow{A}_1^+\right)^T\boldsymbol{k}\right) \\ & \times \hat{U}_{ge}^2\left(\hat{\boldsymbol{r}} + \hbar\left(\overrightarrow{B}_2^0 - \overrightarrow{B}_1^+\right)^T\boldsymbol{k}, \hat{\boldsymbol{p}} - \hbar\left(\overrightarrow{A}_2^0 - \overrightarrow{A}_1^+\right)^T\boldsymbol{k}\right) \\ & \times \hat{U}_{eg}^1(\hat{\boldsymbol{r}},\hat{\boldsymbol{p}}).\end{aligned} \tag{28}$$

Here, the lower indices of $\hat{\phi}$ indicate the number of the laser pulse, and the upper indices indicate whether the time at the beginning of the pulse ("0") or at the end of the pulse ("+") should be taken, for example, $\hat{\phi}_3^+ = \hat{\phi}(2T+4\tau)$. For $\hat{U}$ the associated laser pulse is given by the upper index.

This expression can be simplified if the "reshaping" effect of the laser pulse can be neglected. In that case the two components of the wavefunction follow two well-defined trajectories (Borrmann effect, [22]) and the operators $\hat{\boldsymbol{r}}$ and $\hat{\boldsymbol{p}}$ in $\hat{U}_{ij}$ can be replaced by their mean value, in which case the operators $\hat{g}_i$ are reduced to mere numerical values.

In the case where all atoms were initially in the ground state with wavefunction $|\Psi_{0,g}\rangle$, the fraction of atoms that are still in the ground state at the end of the interferometer sequence can be calculated as:

$$\begin{aligned}P_{gg} = {} & \langle\Psi_{0,g}|\hat{U}_{MZ,gg}^\dagger\hat{U}_{MZ,gg}|\Psi_{0,g}\rangle \\ = {} & \langle\Psi_{0,g}|\hat{g}_1^\dagger\hat{g}_1 + \hat{g}_1^\dagger e^{i\hat{\phi}_{MZ}}\hat{g}_2 + \hat{g}_2^\dagger e^{-i\hat{\phi}_{MZ}}\hat{g}_1 \\ & + \hat{g}_2^\dagger\hat{g}_2|\Psi_{0,g}\rangle.\end{aligned} \tag{29}$$

This is the detection signal, where $\langle\Psi_{0,g}|\hat{g}_1^\dagger e^{i\hat{\phi}_{MZ}}\hat{g}_2|\Psi_{0,g}\rangle + c.c.$ describes the interference fringes and the two terms $g_i^\dagger g_i$ give the offset.

2.5 Short pulse limit

In the short pulse limit $\tau \to 0$, we can drop the superscripts 0 and + in the phase operators and simplify the interferometer phase to

$$\hat{\phi}_{MZ,sp} = \hat{\phi}_1 + \hat{\phi}_3 - 2\hat{\phi}_2 - \frac{i}{2}[\hat{\phi}_1, \hat{\phi}_3 - 2\hat{\phi}_2]. \tag{30}$$

This can be simplified further by filling in the expression for $\hat{\phi}$ (see (16)). Then, using $\overrightarrow{A}_1 = 1$ and $\overrightarrow{B}_1 = 0$, we get for the total phase

$$\begin{aligned}\hat{\phi}_{MZ,sp} = {} & \boldsymbol{k}\cdot\left(\overrightarrow{A}_1 - 2\overrightarrow{A}_2 + \overrightarrow{A}_3\right)\hat{\boldsymbol{r}} \\ & + \boldsymbol{k}\cdot\left(\overrightarrow{B}_1 - 2\overrightarrow{B}_2 + \overrightarrow{B}_3\right)\left(\hat{\boldsymbol{p}} + \frac{\hbar\boldsymbol{k}}{2}\right) \\ & + \boldsymbol{k}\cdot\left(\boldsymbol{\xi}_1 - 2\boldsymbol{\xi}_2 + \boldsymbol{\xi}_3\right) + (\theta_1 - 2\theta_2 + \theta_3).\end{aligned} \tag{31}$$

In the case of a Gaussian initial spatial distribution with an overall momentum, the phase is simply obtained by replacing the operators $\hat{\boldsymbol{r}}$ and $\hat{\boldsymbol{p}}$ with their initial expectation value. This is the result that was obtained in [32] where it is

shown that this expression evaluates to the familiar expressions for the gravimeter and gyroscope configurations. This short pulse limit is completely equivalent to an approach based on the classical trajectories [24, 35].

3 Phase calculations

The full interference signal can be calculated from (29). From this equation we define the interferometer phase Φ_{int} and the amplitude of the interference fringes A_{int} as follows:

$$\Phi_{\text{int}} = \arg\big(\langle\Psi_{0,g}|\hat{g}_1^\dagger e^{i\hat{\phi}_{MZ}}\hat{g}_2|\Psi_{0,g}\rangle\big), \tag{32}$$

$$A_{\text{int}} = 2\big|\langle\Psi_{0,g}|\hat{g}_1^\dagger e^{i\hat{\phi}_{MZ}}\hat{g}_2|\Psi_{0,g}\rangle\big|. \tag{33}$$

In the case of a Gaussian initial wavefunction, it is possible to find an analytic expression for this phase and amplitude. However, even in this simplified example the solution is, in general, unmanageable and we will limit ourselves to a numerical example.

3.1 Parameters

We calculate the phases for a 10 m high gravimeter [16] where we only include the gravitational field and rotation of the Earth. The gravitational acceleration $\boldsymbol{g}$ ($g = 9.8$ m/s^2) is along the z-axis, and the x-axis is chosen such that $\Omega_x = 0$ (see Fig. 1, $\Omega_y = 5.5 \times 10^{-5}$ s^{-1}, $\Omega_z = 4.8 \times 10^{-5}$ s^{-1} at 41° latitude). For the gravitational gradient $\overrightarrow{\overrightarrow{\Gamma}}$ we take the field of a perfectly spherical earth $2\Gamma_{xx} = 2\Gamma_{yy} = -\Gamma_{zz} = 2g_z/R$, where $R = 6.38 \times 10^6$ m is the radius of the Earth and all other components of $\overrightarrow{\overrightarrow{\Gamma}}$ are zero. For the atomic parameters we will take the values of rubidium ($m = 1.44 \times 10^{-25}$ kg).

The atoms interact with two counterpropagating lasers with slightly different frequencies that are tuned so that two ground state levels are resonantly coupled through a far detuned upper level (Raman transition). This way we still have an effective two level system but can transfer the momentum of two photons. The total transferred momentum corresponds to a single photon transition with wavelength $\lambda_{\text{eff}} = 390$ nm. The direction of the laser wavevector is along the z-axis. We will assume that the intensity of the pulses is perfectly matched to their length so that $\Omega_R = \pi/2\tau$. The atoms are launched with a velocity $v_{z0} = -g_z T$. Then, with a separation between pulses $T = 1.43$ s, the atoms reach a maximum height of 10 m. The general expression for the initial momentum is

$$\boldsymbol{p}_0 = m\big(\boldsymbol{v}_0 - \overrightarrow{\Omega}\,(\boldsymbol{r}_0 + \boldsymbol{R})\big); \tag{34}$$

however, in this work we set the initial offset position $\boldsymbol{r}_0$ to zero.

The Raman laser pulses are exactly on resonance (effective detuning $\Delta_l = 0$) at the beginning of the interferometer sequence. Because of the curved trajectory, however, the Doppler shift gives a continuous chirp to the effective detuning and quickly brings the atoms out of resonance. Without adjustment of the laser frequency, the (effective) laser detuning at the second pulse would be too large, there would be no momentum transfer and hence the interferometer would not work. To minimize this effect, it is assumed that at the beginning of each pulse the laser frequency is adjusted to compensate for the Doppler shift that is associated with the classical velocity at that moment. In this example, we compensate for the unperturbed classical trajectory (free fall without lasers) of the atoms (the dot indicates a time derivative):

$$\Delta_i = \Delta_l - \boldsymbol{k}\cdot\big(\dot{\overrightarrow{A}}(t_i)\boldsymbol{r}_0 + \dot{\overrightarrow{B}}(t_i)\boldsymbol{p}_0 + \dot{\boldsymbol{\xi}}(t_i)\big). \tag{35}$$

Changing the laser frequency during the interferometer sequence keeps the effective detuning small and the used Dyson expansion (see (21)) of the interferometer propagator valid. However, it also changes the laser offset phase ϕ_0 from pulse to pulse. It can readily be shown that this adds a phase to the interferometer signal:

$$\phi_{\text{tune}} = \int_\tau^{T+\tau} \Delta_l(t)\,dt - \int_{T+3\tau}^{2T+3\tau} \Delta_l(t)\,dt. \tag{36}$$

This phase is independent of the laser frequency during the pulses and we will omit this phase from further calculations. In the experiment, however, this phase has to be known as precisely as the intended resolution of the measurement and thus requires careful tracking of the laser phase.

3.2 Full wavefunction integral

In this section, we will calculate the interferometer signal as given by (32) and (33). To calculate these expectation values we write the operators $\hat{g}_1$, $\hat{g}_2$, and $\hat{\phi}_{MZ}$ in terms of linear combinations of $\hat{\boldsymbol{r}}$ and $\hat{\boldsymbol{p}}$ and use known eigenvectors of such combinations (see Appendix B). Next we insert the identity

$$1 \equiv \int_\infty^\infty d\boldsymbol{p}^3\,|\phi(\boldsymbol{p})\rangle\langle\phi(\boldsymbol{p})| \tag{37}$$

in front of each combination of $\hat{\boldsymbol{r}}$ and $\hat{\boldsymbol{p}}$, where $|\phi(\boldsymbol{p})\rangle$ is an associated eigenvector, to transform the wavefunction to the basis of these eigenvectors. With this transformation we can treat the subsequent operators as normal functions of the vectors $\boldsymbol{p}$. The cost of these transformations is the introduction of overlap integrals, but these evaluate to simple Gaussians (Appendix B, (63)).

To limit the number of these transformations, we approximate the phase derivatives that we need to evaluate the laser

Table 1 Estimates of the change in laser phase during a laser pulse, broken up into terms of the series expansion in pulse length and in the contributions from $\overset{\Rightarrow}{A}$, $\overset{\Rightarrow}{B}$, and $\boldsymbol{\xi}$. Values are given for 100 μs pulse lengths, position $r = \sigma_r = 50$ μm, and momentum $p = \sigma_p = \hbar/\sigma_r$

Expansion order in τ	$\int_0^\tau \lvert\overset{\Rightarrow}{A}^T\boldsymbol{k}\rvert\sigma_r\, dt$	$\int_0^\tau \lvert\overset{\Rightarrow}{B}^T\boldsymbol{k}\rvert\sigma_p\, dt$	$\int_0^\tau \boldsymbol{k}\cdot\dot{\boldsymbol{\xi}}\, dt$
1	4.4×10^{-7}	2.3×10^{-3}	2.3×10^{3}
2	2.5×10^{-13}	2.6×10^{-12}	1.6×10^{-2}
3			3.5×10^{-13}

transformation matrices (see $\hat{H}_2$, (20)):

$$\frac{d\hat{\phi}}{dt}(t) \approx \boldsymbol{k}\cdot\left(\overset{\Rightarrow}{A}(t_i)\hat{\boldsymbol{r}} + \overset{\Rightarrow}{B}(t_i)\hat{\boldsymbol{p}} + \dot{\boldsymbol{\xi}}(t_i)\right) + \boldsymbol{k}\cdot\ddot{\boldsymbol{\xi}}(t_i)(t-t_i), \tag{38}$$

where we have added the second derivative of $\boldsymbol{\xi}$ because of its relative size ($\ddot{\boldsymbol{\xi}} \approx \boldsymbol{g}$).

The explicit expression for the time derivative of the phase is only used for the correction terms to the laser interaction. The actual contribution to the interferometer phase is given by the time integral during the pulse length τ. Because the pulses are short compared to the total length of the interferometer sequence, this lower order series expansion of the phase evolution during the pulses suffices for the same accuracy of the calculation. To check the validity of this approximation, Table 1 gives numerical estimates of the contribution of expansion coefficients (with respect to τ) to the correction terms of the laser interaction ($\approx \int d\phi/dt(T)\, dt = \phi(T) + d\phi/dt(T)\tau + \cdots$). In this table each expansion coefficient of the phase is broken up in contributions from $\overset{\Rightarrow}{A}$, $\overset{\Rightarrow}{B}$, and $\boldsymbol{\xi}$. Although the maximum values of the $\overset{\Rightarrow}{A}$ and $\overset{\Rightarrow}{B}$ terms are at infinite position and momentum, the contribution from these large offset position and momentum parts of the wavefunction is minimal and we consider the phase difference at the RMS value of the position and momentum. The numerical values are for an interaction time of 100 μs and an atomic cloud of RMS size $\sigma_r = 50$ μm with an associated momentum spread $\sigma_p = \hbar/2\sigma_r$. The lowest entries indicate the terms that are omitted in the approximation of (38). The table shows that for $\tau = 10^{-4}$ s the phase error for all three components is smaller than 10^{-11} rad, making this approximation highly valid. Obviously, the approximation gets even better for shorter τ.

The overall phase $\hat{\phi}_{MZ}$ (see (31)) can always be written as a linear combination of $\hat{\boldsymbol{r}}$ and $\hat{\boldsymbol{p}}$. The evaluation of this phase then requires only one transformation of eigenvectors regardless of the expansion order of the functions $\overset{\Rightarrow}{A}(t)$, $\overset{\Rightarrow}{B}(t)$, and $\boldsymbol{\xi}(t)$, and in this respect there is no gain in truncating the expansion in t.

The contribution from $\dot{\boldsymbol{\xi}}$ would give a very large phase if it were not exactly compensated for by the laser detuning (see (35)). The second term $\boldsymbol{k}\cdot\ddot{\boldsymbol{\xi}} \approx \boldsymbol{k}\cdot\boldsymbol{g}$, however, also gives a phase that is relatively close to unity, indicating that pulse length $\tau = 10^{-4}$ s is at the limit of the validity of the Dyson expansion (see (21)). Sometimes (e.g., in [36]), the laser frequency is chirped during the pulses to compensate for this large phase term. A very complicated phase evolution of the laser could even compensate the entire $\boldsymbol{k}\cdot\boldsymbol{\xi}$ term, thereby greatly improving the validity of the used expansion. The $\boldsymbol{k}\cdot\overset{\Rightarrow}{A}\hat{\boldsymbol{r}}$ and $\boldsymbol{k}\cdot\overset{\Rightarrow}{B}\hat{\boldsymbol{p}}$ terms, however, vary over the wavefunction and cannot be compensated by a chirped laser frequency. These therefore remain as limiting factors for the accuracy.

With the approximation of the phase derivative (see (38)), the expression for the interferometer phase has 7 operators that are linear combinations of $\hat{\boldsymbol{r}}$ and $\hat{\boldsymbol{p}}$. Together with the transformation equation (37) we get a 21-fold integration of a Gaussian times a polynomial. In terms of the unevaluated laser matrix elements and the unevaluated overlap integrals, this has the form:

$$\begin{aligned}
&\langle\Psi_{0,g}|\hat{g}_1^\dagger e^{i\hat{\phi}_{MZ}}\hat{g}_2|\Psi_{0,g}\rangle \\
&= \int d\boldsymbol{p}_1^3\int d\boldsymbol{p}_2^3\int d\boldsymbol{p}_3^3\int d\boldsymbol{p}_4^3\int d\boldsymbol{p}_5^3\int d\boldsymbol{p}_6^3\int d\boldsymbol{p}_7^3 \\
&\quad\times U_{gg}^1(\boldsymbol{r}_C,\boldsymbol{p}_1)^*\times U_{eg}^2(\boldsymbol{r}_C,\boldsymbol{p}_2)^* \\
&\quad\times U_{ge}^3\left(\boldsymbol{r}_C+\hbar\left(\overset{\Rightarrow}{B}_3^0-\overset{\Rightarrow}{B}_2^+\right)^T\boldsymbol{k},\boldsymbol{p}_3-\hbar\left(\overset{\Rightarrow}{A}_3^0-\overset{\Rightarrow}{A}_2^+\right)^T\boldsymbol{k}\right)^* \\
&\quad\times e^{i\phi_{MZ}(\boldsymbol{r}_C,\boldsymbol{p}_4)} \\
&\quad\times U_{gg}^3\left(\boldsymbol{r}_C+\hbar\left(\overset{\Rightarrow}{B}_2^0-\overset{\Rightarrow}{B}_1^+\right)^T\boldsymbol{k},\boldsymbol{p}_5-\hbar\left(\overset{\Rightarrow}{A}_2^0-\overset{\Rightarrow}{A}_1^+\right)^T\boldsymbol{k}\right) \\
&\quad\times U_{ge}^2\left(\boldsymbol{r}_C+\hbar\left(\overset{\Rightarrow}{B}_2^0-\overset{\Rightarrow}{B}_1^+\right)^T\boldsymbol{k},\boldsymbol{p}_6-\hbar\left(\overset{\Rightarrow}{A}_2^0-\overset{\Rightarrow}{A}_1^+\right)^T\boldsymbol{k}\right) \\
&\quad\times U_{eg}^1(\boldsymbol{r}_C,\boldsymbol{p}_7) \\
&\quad\times\left\langle\Psi_{0,g}|\dot{\phi}(t_1),\boldsymbol{p}_1\right\rangle\left\langle\dot{\phi}(t_1),\boldsymbol{p}_1|\dot{\phi}(t_2),\boldsymbol{p}_2\right\rangle \\
&\quad\times\left\langle\dot{\phi}(t_2),\boldsymbol{p}_2|\dot{\phi}(t_3),\boldsymbol{p}_3\right\rangle\left\langle\dot{\phi}(t_3),\boldsymbol{p}_3|\phi_{MZ},\boldsymbol{p}_4\right\rangle \\
&\quad\times\left\langle\phi_{MZ},\boldsymbol{p}_4|\dot{\phi}(t_3),\boldsymbol{p}_5\right\rangle\left\langle\dot{\phi}(t_3),\boldsymbol{p}_5|\dot{\phi}(t_2),\boldsymbol{p}_6\right\rangle \\
&\quad\times\left\langle\dot{\phi}(t_2),\boldsymbol{p}_6|\dot{\phi}(t_1),\boldsymbol{p}_7\right\rangle\left\langle\dot{\phi}(t_1),\boldsymbol{p}_7|\Psi_{0,g}\right\rangle,
\end{aligned} \tag{39}$$

where the asterisk denotes the complex conjugate. By writing this expectation value in terms of the eigenfunctions (see Appendix B), we can replace $\hat{\boldsymbol{r}}$ with an arbitrary, but fixed offset position $\boldsymbol{r}_C$ (we take $\boldsymbol{r}_C = \boldsymbol{0}$) and $\hat{\boldsymbol{p}}$ with the running integration variable $\boldsymbol{p}_i$. The phase term ϕ_{MZ} is obtained from (26). The eigenfunctions $|\dot{\phi}(t_i),\boldsymbol{p}_j\rangle$ are calculated with (58) and (61), taking $\boldsymbol{v} = \overset{\Rightarrow}{A}^T(t_i)\boldsymbol{k}$, $\boldsymbol{w} = \overset{\Rightarrow}{B}^T(t_i)\boldsymbol{k}$,

and $\boldsymbol{p}_c = \boldsymbol{p}_j$. A similar recipe is applied for $|\phi_{MZ}, \boldsymbol{p}_4\rangle$. Finally, the initial wavefunction is a 3D-Gaussian

$$\langle \boldsymbol{r}|\Psi_{g,0}\rangle = \left(\frac{2}{\pi w_0^2}\right)^{\frac{3}{4}} e^{-(\boldsymbol{r}-\boldsymbol{r}_0)^2/w_0^2 + i\,\boldsymbol{p}_0\cdot\boldsymbol{r}/\hbar}, \tag{40}$$

with waist $w_0 = 2\sigma_{r,0}$, momentum $\boldsymbol{p}_0$ (see (34)) and a possible offset position $\boldsymbol{r}_0$ which in this work is usually taken as zero. This is the optimal initial wavefunction that has minimum uncertainty in $\boldsymbol{r}$ and $\boldsymbol{p}$. In practice, this form is very difficult to obtain and the actual atomic wavefunction has a more complicated form. In that case, the following results that are based on this Gaussian shape can be considered as a limiting case for an optimal interference signal.

4 Results

Although, in principle, (39) can be solved analytically, the solution is too extensive to handle in full symbolic form. We therefore calculated the exact solution of the integral only with numerical values of the parameters. We would like to stress that, although we only performed numerical evaluations of the interferometer signal, the solution is still exact and these calculations should not be confused with numerical approximating algorithms that use some form of discretization.

We repeated this calculation for various values of the pulse length and the initial RMS cloud radius $\sigma_{r,0}$. The amplitude and the phase (see (32) and (33)) were then evaluated from the result using symbolic algebra software. The result of the integration is in the form of a large phase in an exponential term (ϕ_{MZ}), multiplied with a complex number with small phase (product of the terms U^i_{jk}). The calculations were performed with 50 digits accuracy and a 5th order expansion of $\vec{A}$, $\vec{B}$, and $\boldsymbol{\xi}$ in t (see (13) and (14)).

The resulting amplitude A_{int} is drawn in Fig. 3 as a function of the initial RMS cloud size $\sigma_{r,0}$. It turns out that the contrast hardly changes with the interaction time and that the graphs are indistinguishable up to 100 μs where the approximations (Expansion (21)) lose their validity. Instead of dependence on τ, the contrast depends much more strongly on $\sigma_{r,0}$ with two boundaries above and below which the amplitude quickly drops to zero. These boundaries correspond to the maximum allowed position spread $\sigma_{r,\max}$ and maximum allowed Heisenberg limited momentum spread $\sigma_{p,\max} = \hbar/2\sigma_{r,\min}$ and can be estimated from the expression of $\hat{\phi}_{MZ}$ (see, e.g., [32] or [35]). They are given by the change in initial position or momentum over which the interferometer phase varies by π. From a leading terms estimate of $\vec{A}$ and $\vec{B}$ we get

$$\sigma_{r,\max} = \frac{\pi}{2k\Gamma T^2} = 1.6\times 10^{-2}\ \text{m}, \tag{41}$$

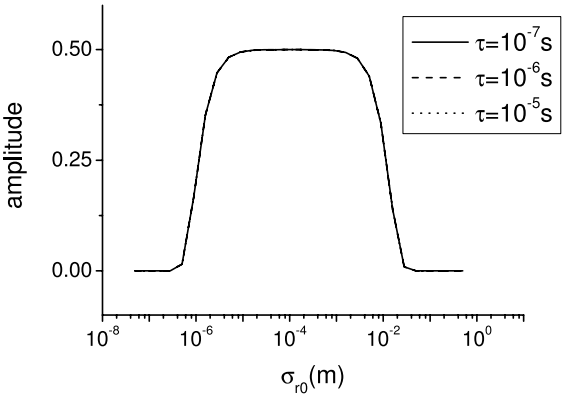

Fig. 3 Amplitude of the interference signal as a function of the initial RMS cloud size $\sigma_{r,0}$

$$\sigma_{r,\min} = \frac{\hbar}{2\sigma_{p,\max}} = \frac{2\hbar k\Omega T^2}{m\pi} = 1.1\times 10^{-6}\ \text{m}. \tag{42}$$

In this case, the criterion on the maximum spread in position originates in the difference in gravity that acts on atoms on opposite sides of the cloud. The other criterion traces back to the difference in Sagnac phase between two atoms that have opposite initial velocity perpendicular to the laser. The numerical values are in good agreement with the graph. Although usually $\sigma_{r,\min} < \sigma_{r,\max}$, it is possible that the restrictions on both the momentum and the position spread are so strong that $\sigma_{r,\min} > \sigma_{r,\max}$, in which case there is no range in which interference fringes can be observed. Note that these limits are obtained from a semiclassical argument, i.e., a straightforward statistical spread of phases over an atomic ensemble. These limits therefore apply as well for a non-coherent and non-Gaussian cloud. In those cases, of course, the momentum spread is not equal to $\hbar/\sigma_{r,0}$ and the first equality of (42) is not valid.

Since in this case the loss of contrast can be explained in a semiclassical way, one can use and expression of the short-pulse phase (like in [35]), which greatly dominates over effects from laser pulse lengths, and estimate the maximum values of most parameters from this.

The phases that are obtained from (39) are plotted in Fig. 4, relative to an offset of approximately 3.2×10^8 rad, as a function of the interaction time τ for several values of $\sigma_{r,0}$. The offset was determined from a linear extrapolation to $\tau = 0$. In this plot, the total time lapse of the interferometer sequence $2T + 4\tau$ was kept constant by compensating the value of T. The actual dependence of the interferometer phase on τ and T is quite complicated and depends on the choice of the laser frequency compensation [22]. For our choice (compensated in steps between laser pulses) that paper predicts a phase in a homogeneous gravitational field of

$$\begin{aligned}\Delta\phi &= \boldsymbol{k}\cdot\boldsymbol{g}\big(T(T+2\tau)+\tau^2/\pi\big)\\ &= \boldsymbol{k}\cdot\boldsymbol{g}(T+\tau)^2 + O\big(\tau^2\big).\end{aligned} \tag{43}$$

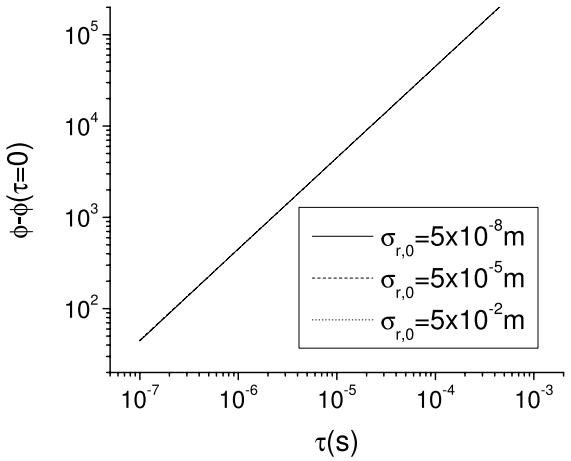

Fig. 4 Double logarithmic plot of the interferometer phase relative to an extrapolated offset phase at $\tau = 0$ s as a function of τ

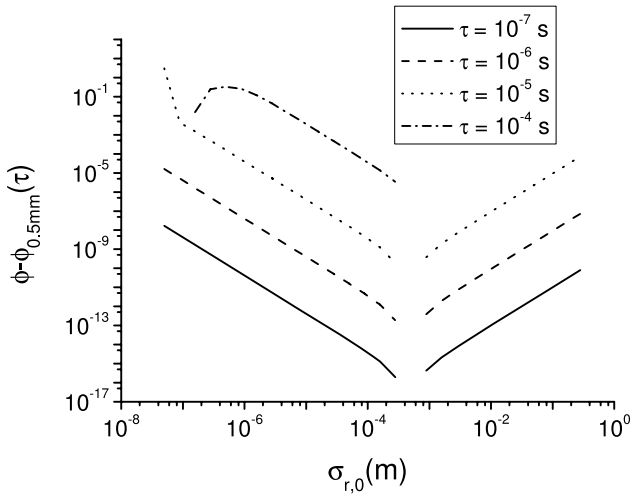

Fig. 5 Interferometer phase relative to the phase for $\sigma_{r,0} = 0.5$ mm (Fig. 4)

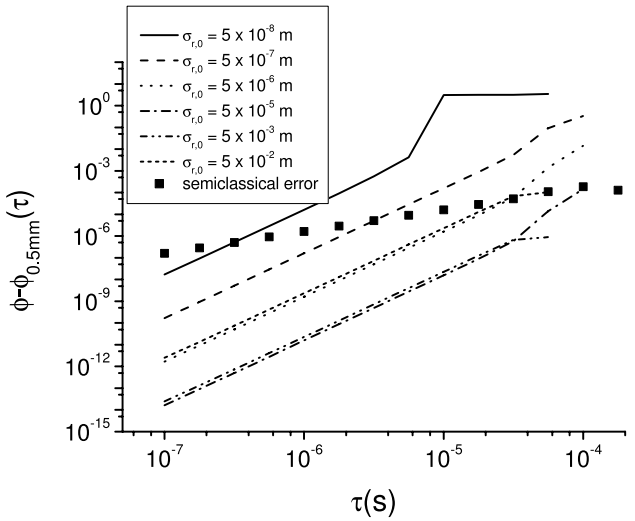

Fig. 6 Interferometer phase relative to the phase for $\sigma_{r,0} = 0.5$ mm (Fig. 4). As a reference the phase error from a semiclassical approximation is plotted as well

Since the dominant effect in our example is gravity, the τ dependence of the phase should closely match this equation. Comparing (43) with a linear fit through the full calculations indicates that the relative difference in the slope ($d\phi/d\tau = 4.50 \times 10^8\ \mathrm{s}^{-1}$) is only 2×10^{-3}, indicating that the model of [22] is indeed a very good approximation for this example. The difference in the phase at $\tau = 0$ is relatively large because of the rotation and the gravity gradient. The remaining difference in the effect of τ between the calculations and (43) is 7 rad for 10 µs pulse length which gives a relative error of 10^{-7}. This difference is mostly caused by presence of rotation during the laser pulses [23].

Equation (43) suggests that the interferometer phase is (approximately) constant if we compensate the length between pulses such that $T + \tau$ is constant. This was verified in a separate set of calculations where we changed the compensation $T + \epsilon\tau = constant$ and indeed found that the phase did no longer change with τ if $\epsilon = 1.0 \pm 0.2$.

The behavior of the phase as a function of τ for other values of $\sigma_{r,0}$, within the explored range (1 m to 50 nm), is indistinguishable from Fig. 4. Therefore, we will take the interferometer phase $\phi_{0.5\,\mathrm{mm}}(\tau)$ for an initial waist of 0.5 mm as a reference for the following graphs and consider the differences with this reference only. This value is arbitrary, in principle, but was chosen for plotting convenience.

In Fig. 5 the interferometer phase relative to the reference $\phi_{0.5\,\mathrm{mm}}(\tau)$ is plotted as a function of $\sigma_{r,0}$ for various values of the interaction time τ. The plot shows that there is a minimum in the phase at $\sigma_{r,0} = 0.5$ mm for all interaction times τ. For larger initial clouds the interferometer phase increases with $\sigma_{r,0}^2$ and for smaller $\sigma_{r,0}$ the phase goes with $1/\sigma_{r,0}^2$. We can understand both the existence of the shift and the quadratic behavior by considering the average value of a phase operator over a symmetric wavefunction. Because of the spatial (and momentum) dependence of the phase there will be a larger phase difference if the wavefunction is broad (narrow). The large phase variation over the cloud will then introduce an average phase shift. Because the wavefunction is symmetric, all contributions that are odd in position will cancel out in the average and the dominant contribution to the phase shift is quadratic in position/momentum spread. The phase minimum is at the point where the contributions from the size and the momentum spread are equal. Experimentally, this cloud size is the best to choose because then the sensitivity to changes in cloud size is minimal.

The graph also clearly shows that a shorter interaction time gives less effect of $\sigma_{r,0}$ on the phase. In the limit $\tau \to 0$, we return to the short pulse limit in which there is no effect of the initial cloud size at all. This is further illustrated by Fig. 6 where the same data is now plotted as a function of τ.

According to this graph, the phase (relative to the reference $\phi_{0.5\,\mathrm{mm}}(\tau)$) grows approximately with τ^3 for all values of the initial RMS cloud size and over the entire plotted range of τ. At $\tau = 100$ µs the phase term $\boldsymbol{k}\cdot\boldsymbol{g}\tau^2 \approx 1$. Then the used expansion (see (21)) is no longer valid which causes the jumps in phase and the missing points (in the logarithmic scale).

As a reference, we also calculated the phase that results from (29) if the operators $\hat{\boldsymbol{r}}$ and $\hat{\boldsymbol{p}}$ are simply replaced by their initial expectation value $\boldsymbol{r}_0$ and $\boldsymbol{p}_0$. In effect this means substituting the classical trajectories and neglecting the wavefront distortion by the beamsplitter (Borrmann effect). The difference between this and the full quantum calculation for $\sigma_{r,0} = 5 \times 10^{-4}$ m is also plotted in Fig. 6. Again, this reference is arbitrary as the semiclassical phase does not depend on the shape of the initial wavefunction. The plot shows that the error in the semiclassical approximation increases approximately linear with τ. For typical experimental parameters this simplified calculation introduces an of $\sim 10^{-5}$ rad.

5 Outlook

In this work, we were able to calculate the interferometer signal with a very high precision using a series of transformations. These calculations are very general and can be applied or straightforwardly extended to a large number of situations. The generality lies mostly in the fact that it accounts for a large range of inertial fields and potentials, rotation and even space–time curvature [37]. The only assumption that we made was that the resulting change in Doppler shift during the pulses were small compared to the Rabi frequency. We have shown the result for a perfectly symmetric Mach–Zehnder interferometer, but the effect of errors in timing can easily be evaluated with different numerical values of the parameters. The presented method is not valid (with the same accuracy) for spatial interferometers, which require a different approach [38]. However, the signal of many more complicated interferometer configurations or the inclusion of spontaneous emission between laser pulses can be calculated by straightforward introduction of additional laser pulse operators.

In the calculations presented here we took the Rabi frequency constant and homogeneous. If this is not the case, for example, because of finite switching time or a spatially finite (Gaussian) laser beam, one can no longer take an interaction picture relative to an unperturbed Rabi oscillation (see (20)) and the Rabi oscillations will have to be evaluated in a perturbative way (e.g., Dyson expansion). In that case, however, the accuracy of the calculations will be strongly limited as $\Omega_R\tau \sim 1$ ($\pi/4$ in the ideal case) such that τ can no longer be used as an expansion parameter. Similarly, higher order terms in the potential/intertial field can be added in a perturbative way. These effects, however, are integrated over long times T and must be very small to have a converging expansion.

Under the assumption that the total population of one atomic level over the entire space is measured, it is not necessary to transform the final wavefunction back to the original reference frame. If one is interested in the spatial profile of the final wavefunction, e.g., because of a finite detection area, the result after application of $\hat{U}_{MZ,gg}$ has to be multiplied with another transformation operator. Evaluation of the wavefunction then requires an expansion into Hermite–Gaussians [30].

The big advantage of the used method is that for a simple Gaussian initial wave equation (39) can be solved exactly. This avoids the use of approximating/discretizing numerical algorithms that reduce the accuracy of the result and for which it may be difficult to get a converging result because of the fast spatial oscillation (momentum). This solvability is lost quickly if the initial state is more complicated. However, there are some examples that do have an analytic solution. One can think, for example, of an MOT with a Gaussian position and momentum distribution. This would require calculating the interference signal as described in this work and then average this signal (incoherently) over the momentum distribution. This adds one more integration to (39). Similarly, the signal of a wavefunction with two coherent Gaussians can be calculated. This, however, requires calculating the cross terms between the two final states as well which adds a second integration/summation step to the calculation.

6 Conclusions

We have calculated the interferometer phase in a realistic interferometer, taking into account the finite length of the laser pulses and the associated distortion of the atomic wavefunction. Comparison with existing expressions shows a discrepancy of approximately 1 rad, which in the considered setup is a relative error of 10^{-8}. Although it is interesting to see how accurate these existing expressions are, it is no surprise that there is a difference as they are based on first-order expansions. Likely, the accuracy of these models can straightforwardly be improved by including higher orders, as illustrated by the semiclassical calculations in Fig. 6.

The main result of this work, however, is the effect of the shape of the initial wavefunction on the final interferometer phase. We have shown that this effect can shift the interferometer phase by 10^{-5} rad (10^{-13} relative error), or more, for typical experimental parameters. Table 2 shows the accuracy of some state of the art interferometers. These have various configurations and measure different quantities, so

Table 2 Some relative uncertainties in atom interferometer experiments

Measured effect	Relative uncertainty
Gravitational acceleration [3]	10^{-9}
Equivalence principle, proposal [16]	10^{-15}
Newtonian gravitational constant [14, 15]	10^{-3}
Rotation [7]	10^{-4} (in 1 s)
Electric polarizability [11, 12]	10^{-3}
Transition frequency [9, 10]	10^{-16}

it is difficult to compare these among each other or with the example in this work. The table does show, however, that some of these experiments are in the range of the calculated phase errors and have to take the wavefront distortion by the laser pulses into account with the interpretation of their signal.

Appendix A: Atom interferometer

In the two-path approximation the total interferometer evolution operator is given by

$$\begin{aligned}\hat{U}_{MZ} &= \hat{U}_{\text{laser}}(2T+3\tau,\tau)\hat{U}_{\text{laser}}(T+\tau,2\tau)\hat{U}_{\text{laser}}(0,\tau)\\ &= \begin{pmatrix} e^{i\hat{\phi}_3^+}\hat{U}^3_{ee}e^{-i\hat{\phi}_3^0} & e^{i\hat{\phi}_3^+}\hat{U}^3_{eg}\\ \hat{U}^3_{ge}e^{-i\hat{\phi}_3^0} & \hat{U}^3_{gg}\end{pmatrix}\\ &\quad\times\begin{pmatrix} 0 & e^{i\hat{\phi}_2^+}\hat{U}^2_{eg}\\ \hat{U}^2_{ge}e^{-i\hat{\phi}_2^0} & 0\end{pmatrix}\\ &\quad\times\begin{pmatrix} e^{i\hat{\phi}_1^+}\hat{U}^1_{ee}e^{-i\hat{\phi}_1^0} & e^{i\hat{\phi}_1^+}\hat{U}^1_{eg}\\ \hat{U}^1_{ge}e^{-i\hat{\phi}_1^0} & \hat{U}^1_{gg}\end{pmatrix}\\ &= \begin{pmatrix} e^{i\hat{\phi}_3^+}\hat{U}^3_{ee}e^{-i\hat{\phi}_3^0}e^{i\hat{\phi}_2^+} & e^{i\hat{\phi}_3^+}\hat{U}^3_{ee}e^{-i\hat{\phi}_3^0}\\ \times\hat{U}^2_{eg}\hat{U}^1_{ge}e^{-i\hat{\phi}_1^0} & \times e^{i\hat{\phi}_2^+}\hat{U}^2_{eg}\hat{U}^1_{gg}\\ +e^{i\hat{\phi}_3^+}\hat{U}^3_{eg}\hat{U}^2_{ge}e^{-i\hat{\phi}_2^0} & +e^{i\hat{\phi}_3^+}\hat{U}^3_{eg}\hat{U}^2_{ge}\\ \times e^{i\hat{\phi}_1^+}\hat{U}^1_{ee}e^{-i\hat{\phi}_1^0} & \times e^{-i\hat{\phi}_2^0}e^{i\hat{\phi}_1^+}\hat{U}^1_{eg}\\ \hat{U}^3_{ge}e^{-i\hat{\phi}_3^0}e^{i\hat{\phi}_2^+} & \hat{U}^3_{ge}e^{-i\hat{\phi}_3^0}e^{i\hat{\phi}_2^+}\\ \times\hat{U}^2_{eg}\hat{U}^1_{ge}e^{-i\hat{\phi}_1^0} & \times\hat{U}^2_{eg}\hat{U}^1_{gg}\\ +\hat{U}^3_{gg}\hat{U}^2_{ge}e^{-i\hat{\phi}_2^0} & +\hat{U}^3_{gg}\hat{U}^2_{ge}e^{-i\hat{\phi}_2^0}\\ \times e^{i\hat{\phi}_1^+}\hat{U}^1_{ee}e^{-i\hat{\phi}_1^0} & \times e^{i\hat{\phi}_1^+}\hat{U}^1_{eg}\end{pmatrix},\end{aligned}\tag{44}$$

$$t_1=0,\qquad t_2=T+\tau,\qquad t_3=2T+3\tau,\tag{45}$$

$$\tau_1=\tau_3=\tau,\qquad \tau_2=2\tau,\tag{46}$$

$$\hat{U}^k_{ij}=\hat{U}_{ij}(t_k,\tau_k,\hat{\boldsymbol{r}},\hat{\boldsymbol{p}}),\tag{47}$$

$$\hat{\phi}^0_k=\hat{\phi}(t_k,\hat{\boldsymbol{r}},\hat{\boldsymbol{p}}),\qquad \hat{\phi}^+_k=\hat{\phi}(t_k+\tau_k,\hat{\boldsymbol{r}},\hat{\boldsymbol{p}}).\tag{48}$$

The operator that describes the transition from ground state to ground state is the lower right element:

$$\begin{aligned}\hat{U}_{MZ,gg} &= \hat{U}^3_{ge}(\hat{\boldsymbol{r}},\hat{\boldsymbol{p}})e^{-i\hat{\phi}^0_3}e^{i\hat{\phi}^+_2}\hat{U}^2_{eg}(\hat{\boldsymbol{r}},\hat{\boldsymbol{p}})\hat{U}^1_{gg}(\hat{\boldsymbol{r}},\hat{\boldsymbol{p}})\\ &\quad+\hat{U}^3_{gg}(\hat{\boldsymbol{r}},\hat{\boldsymbol{p}})\hat{U}^2_{ge}(\hat{\boldsymbol{r}},\hat{\boldsymbol{p}})e^{-i\hat{\phi}^0_2}e^{i\hat{\phi}^+_1}\hat{U}^1_{eg}(\hat{\boldsymbol{r}},\hat{\boldsymbol{p}}),\end{aligned}\tag{49}$$

where we have added the $\hat{\boldsymbol{r}}$ and $\hat{\boldsymbol{p}}$ dependence in the functions $\hat{U}_{ij}$ explicitly because they have to be replaced when the exponentials in $\hat{U}_{MZ,gg}$ are rearranged. To get one single phase operator we combine the exponential terms using the relations [39, 40]

$$e^{\hat{A}}\hat{B}e^{-\hat{A}}=\hat{B}+[\hat{A},\hat{B}]+\frac{1}{2!}\big[\hat{A},[\hat{A},\hat{B}]\big]+\cdots,\tag{50}$$

$$\begin{aligned}e^{\hat{A}+\hat{B}} &= e^{\hat{A}}e^{\hat{B}}e^{-\frac{1}{2}[\hat{A},\hat{B}]}\\ &\text{if }\big[\hat{A},[\hat{A},\hat{B}]\big]=\big[\hat{B},[\hat{A},\hat{B}]\big]=0\end{aligned}\tag{51}$$

between two operators $\hat{A}$ and $\hat{B}$, and the derived relation

$$e^{\boldsymbol{v}\cdot\hat{\boldsymbol{r}}+\boldsymbol{w}\cdot\hat{\boldsymbol{p}}}f(\hat{\boldsymbol{r}},\hat{\boldsymbol{p}})=f(\hat{\boldsymbol{r}}-i\hbar\boldsymbol{w},\hat{\boldsymbol{p}}+i\hbar\boldsymbol{v})e^{\boldsymbol{v}\cdot\hat{\boldsymbol{r}}+\boldsymbol{w}\cdot\hat{\boldsymbol{p}}}\tag{52}$$

for a general function f. We obtain

$$\begin{aligned}\hat{U}_{MZ,gg} &= e^{-i\hat{\phi}^0_3}e^{i\hat{\phi}^+_2}\\ &\quad\times\hat{U}^3_{ge}\big(\hat{\boldsymbol{r}}+\hbar\big(\overrightarrow{\overrightarrow{B}}^0_3-\overrightarrow{\overrightarrow{B}}^+_2\big)^T\boldsymbol{k},\\ &\qquad\hat{\boldsymbol{p}}-\hbar\big(\overrightarrow{\overrightarrow{A}}^0_3-\overrightarrow{\overrightarrow{A}}^+_2\big)^T\boldsymbol{k}\big)\\ &\quad\times\hat{U}^2_{eg}(\hat{\boldsymbol{r}},\hat{\boldsymbol{p}})\hat{U}^1_{gg}(\hat{\boldsymbol{r}},\hat{\boldsymbol{p}})\\ &\quad+e^{-i\hat{\phi}^0_2}e^{i\hat{\phi}^+_1}\\ &\quad\times\hat{U}^3_{gg}\big(\hat{\boldsymbol{r}}+\hbar\big(\overrightarrow{\overrightarrow{B}}^0_2-\overrightarrow{\overrightarrow{B}}^+_1\big)^T\boldsymbol{k},\\ &\qquad\hat{\boldsymbol{p}}-\hbar\big(\overrightarrow{\overrightarrow{A}}^0_2-\overrightarrow{\overrightarrow{A}}^+_1\big)^T\boldsymbol{k}\big)\\ &\quad\times\hat{U}^2_{ge}\big(\hat{\boldsymbol{r}}+\hbar\big(\overrightarrow{\overrightarrow{B}}^0_2-\overrightarrow{\overrightarrow{B}}^+_1\big)^T\boldsymbol{k},\\ &\qquad\hat{\boldsymbol{p}}-\hbar\big(\overrightarrow{\overrightarrow{A}}^0_2-\overrightarrow{\overrightarrow{A}}^+_1\big)^T\boldsymbol{k}\big)\\ &\quad\times\hat{U}^1_{eg}(\hat{\boldsymbol{r}},\hat{\boldsymbol{p}})\\ &\equiv e^{-i\hat{\phi}^0_3}e^{i\hat{\phi}^+_2}\hat{g}_1+e^{-i\hat{\phi}^0_2}e^{i\hat{\phi}^+_1}\hat{g}_2,\end{aligned}\tag{53}$$

$$\overrightarrow{\overrightarrow{A}}^0_k=\overrightarrow{\overrightarrow{A}}(t_k),\qquad \overrightarrow{\overrightarrow{A}}^+_k=\overrightarrow{\overrightarrow{A}}(t_k+\tau_k),\tag{54}$$

$$\overrightarrow{\overrightarrow{B}}^0_k=\overrightarrow{\overrightarrow{B}}(t_k),\qquad \overrightarrow{\overrightarrow{B}}^+_k=\overrightarrow{\overrightarrow{B}}(t_k+\tau_k).\tag{55}$$

The operators $\hat{g}_1$ and $\hat{g}_2$, as defined by (53), describe the amplitudes and small phase corrections of the two paths of the interferometer. Using (51) we get an expression for the interferometer propagator

$$\hat{U}_{MZ,gg} = e^{-i\hat{\phi}_3^0} e^{i\hat{\phi}_2^+} \left[\hat{g}_1 + e^{-i\hat{\phi}_{MZ}} \hat{g}_2\right], \tag{56}$$

with the total phase operator

$$\hat{\phi}_{MZ} = \hat{\phi}_1^+ - \hat{\phi}_2^0 - \hat{\phi}_2^+ + \hat{\phi}_3^0 - \frac{i}{2}\left[\left[\hat{\phi}_2^+, \hat{\phi}_3^0\right] + \left[\hat{\phi}_2^0, \hat{\phi}_1^+\right] - \left[\hat{\phi}_2^+ - \hat{\phi}_3^0, \hat{\phi}_1^+ - \hat{\phi}_2^0\right]\right]. \tag{57}$$

Appendix B: Eigenfunctions

According to (29), the interferometer signal is the expectation value of a function of several operators that are a linear combination of $\hat{\boldsymbol{r}}$ and $\hat{\boldsymbol{p}}$. To evaluate this signal it is thus very useful to take a look at the eigenvectors of such an operator $\hat{\phi} = \boldsymbol{v}\cdot\hat{\boldsymbol{r}} + \boldsymbol{w}\cdot\hat{\boldsymbol{p}}$. In the $\boldsymbol{r}$ representation the eigenfunctions, $\phi(\boldsymbol{r}) = \langle \boldsymbol{r}|\phi\rangle$ of this operator are described by a complex valued 3D-Gaussian:

$$\phi(\boldsymbol{r}) = (2\pi\hbar)^{(3/2)} e^{i(\boldsymbol{r}-\boldsymbol{r}_c)\cdot\overrightarrow{W}(\boldsymbol{r}-\boldsymbol{r}_c)+i\boldsymbol{p}_c\cdot\boldsymbol{r}/\hbar}, \tag{58}$$

if

$$\boldsymbol{v} + 2\hbar\overrightarrow{W}^T\boldsymbol{w} = 0 \tag{59}$$

with eigenvalues

$$\Phi = -2\hbar\boldsymbol{w}\cdot\overrightarrow{W}\boldsymbol{r}_c + \boldsymbol{w}\cdot\boldsymbol{p}_c = \boldsymbol{v}\cdot\boldsymbol{r}_c + \boldsymbol{w}\cdot\boldsymbol{p}_c. \tag{60}$$

In the special case that the initial wavefunction is exactly equal to one of these eigenfunctions, the expectation value of any operator that is a function of $\hat{\phi}$ can thus be obtained by simply replacing the operators $\hat{\boldsymbol{r}}$ and $\hat{\boldsymbol{p}}$ with their initial expectation value $\boldsymbol{r}_c$ and $\boldsymbol{p}_c$. In all other cases, one has to average over all eigenfunctions with the appropriate weighting factors.

The matrix $\overrightarrow{W}$, as set by (59), can be obtained from

$$2\hbar\overrightarrow{W}^T = -\frac{\boldsymbol{v}\otimes\boldsymbol{w}^T}{\boldsymbol{w}\cdot\boldsymbol{w}} + \boldsymbol{\alpha}_1\otimes\boldsymbol{w}_{\perp,1}^T + \boldsymbol{\alpha}_2\otimes\boldsymbol{w}_{\perp,2}^T, \tag{61}$$

where the notation $\otimes$ is used for a direct product only to emphasize the difference with the inner product. The vectors $\boldsymbol{w}_{\perp,i}$ are perpendicular to $\boldsymbol{w}$, and the vectors $\boldsymbol{\alpha}_i$ have to be chosen so that $\overrightarrow{W}$ is symmetric.

One can create a complete set of eigenfunctions with the free parameter $\boldsymbol{p}_c$ so that any function can be expanded in terms of these eigenfunctions with coefficients

$$\tilde{f}(\boldsymbol{p}_c) = \int_{-\infty}^{\infty} dr^3 f(\boldsymbol{r}) e^{-i(\boldsymbol{r}-\boldsymbol{r}_c)\overrightarrow{W}(\boldsymbol{r}-\boldsymbol{r}_c)-i\boldsymbol{p}_c\cdot\boldsymbol{r}/\hbar}. \tag{62}$$

For the calculations of the interferometer signal, we will be mostly interested in the transformation of one basis function $|\phi_1\rangle$ to the set of eigenfunctions $\{|\phi_2\rangle\}$ of a different operator $\hat{\phi}$ with different width $\overrightarrow{W}_2$. For this transformation, we have to calculate the overlap between all of these eigenfunctions, which is done by using the $\boldsymbol{r}$ representation (see (58)). There is no restriction on the parameter $\boldsymbol{r}_c$, so we will take this to be zero in the following (this has no effect on the overlap integral):

$$\begin{aligned}
&\langle\phi_1(\boldsymbol{p}_1)|\phi_2(\boldsymbol{p}_2)\rangle \\
&= \int_{-\infty}^{\infty} dr^3 \langle\phi_1(\boldsymbol{p}_1)|\boldsymbol{r}\rangle\langle\boldsymbol{r}|\phi_2(\boldsymbol{p}_2)\rangle \\
&= \int_{-\infty}^{\infty} dr^3 e^{i\boldsymbol{r}\overrightarrow{W}_1\boldsymbol{r}+i\boldsymbol{p}_1\cdot\boldsymbol{r}/\hbar} e^{-i\boldsymbol{r}\overrightarrow{W}_2\boldsymbol{r}-i\boldsymbol{p}_2\cdot\boldsymbol{r}/\hbar} \\
&= \int_{-\infty}^{\infty} dr^3 e^{i\boldsymbol{r}\overrightarrow{W}_{12}\boldsymbol{r}+i\boldsymbol{p}_{12}\cdot\boldsymbol{r}/\hbar} \\
&= \int_{-\infty}^{\infty} dr^3 e^{i(\boldsymbol{r}+\overrightarrow{W}_{12}^{-1}\boldsymbol{p}_{12}/2\hbar)\overrightarrow{W}_{12}(\boldsymbol{r}+\overrightarrow{W}_{12}^{-1}\boldsymbol{p}_{12}/2\hbar)} \\
&\quad\times e^{-i\boldsymbol{p}_{12}\overrightarrow{W}_{12}^{-1}\boldsymbol{p}_{12}/4\hbar^2} \\
&= e^{-i\boldsymbol{p}_{12}\overrightarrow{W}_{12}^{-1}\boldsymbol{p}_{12}/4\hbar^2}\int_{-\infty}^{\infty} dr'^3 e^{i\boldsymbol{r}'\overrightarrow{W}_{12}\boldsymbol{r}'} \\
&= e^{-i\boldsymbol{p}_{12}\overrightarrow{W}_{12}^{-1}\boldsymbol{p}_{12}/4\hbar^2}\left(\det\overrightarrow{W}_{12}\right)^{-1/2}\int_{-\infty}^{\infty} dr''^3 e^{i\boldsymbol{r}''\cdot\boldsymbol{r}''} \\
&= e^{-i\boldsymbol{p}_{12}\overrightarrow{W}_{12}^{-1}\boldsymbol{p}_{12}/4\hbar^2}\left(\det\overrightarrow{W}_{12}\right)^{-1/2}(i\pi)^{\frac{3}{2}},
\end{aligned} \tag{63}$$

where the index 12 indicates the difference $1-2$ and det is the determinant of the matrix.

References

1. P.R. Berman (ed.), *Atom Interferometry* (Academic, New York, 1997)
2. J. Baudon, R. Mathevet, J. Robert, J. Phys. B **32**, R173 (1999)
3. A. Peters, K.Y. Chung, S. Chu, Nature **400**, 849 (1999)
4. A. Peters, *High Precision Gravity Measurements Using Atom Interferometery*, Ph.D. thesis, Stanford University, 1998
5. J.F. Clauser, Physica B **151**, 262 (1988)
6. F. Riehle, T. Kisters, A. Witte, J. Helmcke, C.J. Bordé, Phys. Rev. Lett. **67**, 177 (1991)
7. T.L. Gustavson, P. Bouyer, M.A. Kasevich, Phys. Rev. Lett. **78**, 2046 (1997)
8. G. Wilpers, T. Binnewies, C. Degenhardt, U. Sterr, J. Helmcke, F. Riehle, Phys. Rev. Lett. **89**, 230801 (2002)
9. A.D. Ludlow, T. Zelevinsky, G.K. Campbell, S. Blatt, M.M. Boyd, M.H.G. de Miranda, M.J. Martin, J.W. Thomsen, S.M. Foreman, J. Ye, T.M. Fortier, J.E. Stalnaker, S.A. Diddams, Y. Le Coq, Z.W. Barber, N. Poli, N.D. Lemke, K.M. Beck, C.W. Oates, Science **319**, 1805 (2008)
10. T. Rosenband, D.B. Hume, P.O. Schmidt, C.W. Chou, A. Brusch, L. Lorini, W.H. Oskay, R.E. Drullinger, T.M. Fortier, J.E. Stalnaker, S.A. Diddams, W.C. Swann, N.R. Newbury, W.M. Itano, D.J. Wineland, J.C. Bergquist, Science **319**, 1808 (2008)

11. C.R. Ekstrom, J. Schmiedmayer, M.S. Chapman, T.D. Hammond, D.E. Pritchard, Phys. Rev. A **51**, 3883 (1995)
12. A. Miffre, M. Jacquey, M. Büchner, G. Trénec, J. Vigué, Phys. Rev. A **73**, 011603(R) (2006)
13. A. Wicht, J.M. Hensley, E. Sarajlic, S. Chu, Phys. Scr. T **102**, 82 (2002)
14. J.B. Fixler, G.T. Foster, J.M. McGuirk, M.A. Kasevich, Science **315**, 74 (2007)
15. G. Lamporesi, A. Bertoldi, L. Cacciapuoti, M. Prevedelli, G.M. Tino, Phys. Rev. Lett. **100**, 050801 (2008)
16. S. Dimopoulos, P.W. Graham, J.M. Hogan, M.A. Kasevich, Phys. Rev. Lett. **98**, 111102 (2007)
17. C. Jentsch, T. Müller, E.M. Rasel, W. Ertmer, Gen. Relativ. Gravit. **36**, 2197 (2004)
18. C. Lämmerzahl, *Atom Beam Interferometry, Atom Optics, and Gravitation*, Habilitation Thesis, University of Konstanz, 1997
19. C. Antoine, *Contribution á la théorie des interféromètres atomique*, Ph.D. thesis, Université Pierre et Marie Curie, Paris, 2004
20. P. Cheinet, B. Canuel, F. Pereira dos Santos, A. Gauguet, F. Yver-LeDuc, A. Landragin, IEEE Trans. Inst. Meas. **57**, 1141 (2008)
21. C.J. Bordé, Metrologia **39**, 435 (2002)
22. C. Antoine, Appl. Phys. B **84**, 585 (2006)
23. C. Antoine, Phys. Rev. A **76**, 033609 (2007)
24. P. Storey, C. Cohen-Tannoudji, J. Phys. II **4**, 1999 (1994)
25. C. Chiu, L. Stodolsky, Phys. Rev. D **22**, 1337 (1980)
26. P.Y. Zhu, Z.J. Shen, Y.S. Wu, Phys. Rev. D **32**, 368 (1985)
27. J. Audretsch, K.P. Marzlin, J. Phys. **4**, 2073 (1994)
28. B. Young, M. Kasevich, S. Chu, in *Atom Interferometry*, ed. by P. Berman (Academic, New York, 1997), p. 366
29. D.M. Giltner, R.W. McGowan, S.A. Lee, Phys. Rev. A **52**, 3966 (1995)
30. C.J. Bordé, Propagation of Laser Beams and of Atomic Systems, Les Houches Lectures, Session LIII, 1990
31. M.A.H.M. Jansen, *Atom Interferometry with Cold Metastable Helium*, Ph.D. thesis, Eindhoven University of Technology, 2007
32. C.J. Bordé, J. Opt. B: Quant. Semiclass. Opt. **5**, S199 (2003)
33. C. Lämmerzahl, C.J. Bordé, Phys. Lett. A **203**, 59 (1995)
34. K.P. Marzlin, J. Audretsch, Phys. Rev. A **53**, 1004 (1996)
35. K. Bongs, R. Launay, M.A. Kasevich, Appl. Phys. B **84**, 599 (2006)
36. M. Kasevich, S. Chu, Appl. Phys. B **54**, 321 (1992)
37. Ch.J. Bordé, Gen. Relativ. Gravit. **36**, 475 (2004)
38. Ch.J. Bordé, Ann. Phys. (Leipzig) **8**, 83 (1999)
39. B.G. Adams, *Algebraic Approach to Simple Quantum Systems* (Springer, Berlin, 1994), p. 18
40. C. Cohen-Tannoudji, B. Diu, F. Laloe, *Quantum Mechanics*, vol. 1 (Wiley Interscience, New York, 1977), p. 174